A new portable field rotational viscometer for high-temperature melts

M O Chevrel, T. Latchimy, L. Batier, Romain Delpoux, M. Harris, S. Kolzenburg

Chevrel MO, Latchimy T, Batier L, Delpoux R, Harris M, Kolzenburg S. A new portable field rotational viscometer for high-temperature melts. Rev Sci Instrum. 2023 Oct 1;94(10):105116. doi: 10.1063/5.0160247.

A new portable field rotational viscometer for high-temperature melts

M. O. Chevrel[1,2,3,a)], T. Latchimy[1], L. Batier[4], R. Delpoux[5], M. Harris[6], S. Kolzenburg[6]

[1]*Université Clermont Auvergne, CNRS, IRD, OPGC, Laboratoire Magmas et Volcans, 63000 Clermont-Ferrand, France.*
[2]*Université Paris Cité, Institut de physique du globe de Paris, CNRS, 75005 Paris, France*
[3]*Observatoire volcanologique du Piton de la Fournaise, Institut de physique du globe de Paris, 97418 La Plaine des Cafres, France*
[4]*Université Clermont Auvergne, Polytech Clermont, 63000 Clermont-Ferrand, France.*
[5]*Univ Lyon, INSA Lyon, Université Claude Bernard Lyon 1, Ecole Centrale de Lyon, CNRS, Ampère, UMR5005, 69621 Villeurbanne, France*
[6]*Department of Geology University at Buffalo, 126 Cooke Hall Buffalo, NY 14260-4130, USA*

a) Author to whom correspondence should be addressed: oryaelle.chevrel@ird.fr

ABSTRACT

Mounted on top of furnaces, laboratory viscometers can be used for the rheological characterization of high temperature melts, such as molten rocks (lava). However, there are no instruments capable of measuring the viscosity of large volumes of high temperature melts outside the laboratory at, for example, active lava flows on volcanoes or at industrial sites. In this article, we describe a new instrument designed to be easy to operate, highly mobile, and capable of measuring the viscosity of high temperature liquids and suspensions (<1350°C). The device consists of a torque sensor mounted in line with a stainless-steel shear vane that is immersed in the melt and driven by a motor that rotates the shear vane. In addition, a thermocouple placed between the blades of the shear vane measures the temperature of the melt at the measurement location. An onboard microcomputer records torque, rotation rate, and temperature simultaneously and in real time, thus enabling the characterization of the rheological flow curve of the material as a function of temperature and strain rate. The instrument is calibrated using viscosity standards at low temperatures (20-60°C) and over a wide range of stress (30-3870 Pa), strain rate (0.1-27.9 s^{-1}), and viscosity (10-650 Pa·s). High temperature tests were performed in large scale experiments within 25 l of lava at temperatures between 1000 and 1350°C to validate the system s performance for future use in natural lava flows. This portable field viscometer was primarily designed to measure the viscosity of geological melts at their relevant temperatures and in their natural state on the flanks of volcanoes, but it could also be used for industrial purposes and beyond.

I. INTRODUCTION

A. Motivation

Rheological properties govern the mobility of all flowing media and are described within the stress-strain rate space. The rheological properties of all liquids are temperature dependent. As a result, characterizing the thermo-rheological properties is an essential component of geo- and material sciences, and also the food, and other molten material industries. Characterizing geological melts requires working over a wide range of temperatures, with maximum temperatures in excess of 1700 °C for silicate melts, over which viscosity can vary by several orders of magnitude. These variations are even more pronounced for natural volcanic melts and suspensions, such as lava, that have drastically varying viscosities as cooling, degassing, and crystallization occurs. Characterizing viscosity variations is the key to understanding and forecasting volcanic eruption dynamics. Measuring the viscosity as a function of temperature and deformation rate has therefore been one of the major challenges for earth scientists for decades[1–9].

Measuring viscosity is a well-known science and a large range of laboratory viscometers are available. These laboratory viscometers are precise and highly reliable instruments. They can reach an accuracy of better than 0.01 Pa·s and can measure very small quantities of liquid (a few ml). For measuring the viscosity of very high temperature melts (up to 1700 °C), viscometer heads can be placed above a furnace and a heat resistant spindle inserted into the melt[10–12]. However, laboratory measurements, cannot always reproduce natural or industrial conditions, especially in scale. Indeed, there is no commercially available device that can measure the viscosity of large amounts of molten material at volcanoes or in industrial applications.

B. Background on lava viscometry

The rheological properties of lava control lava flow emplacement dynamics including trajectories, velocities, and runout distances. These parameters are used to calibrate numerical models providing support to risk mitigation strategies [13–17]. Since the late 1980s, viscometry in the laboratory has been a common method that works with re-melted lava under a well-controlled environment (temperature, shear rate, oxygen fugacity) and allows for very precise measurements (< 0.01 log Pa·s) [10,18,19]. Over the years these methods have improved to better characterize the rheological properties of melts, but there are still some unknowns. Laboratory experiments are typically able to measure pure melt or two-phase suspensions (melt + crystals). They are, however, unable to completely replicate natural conditions where the content and type of crystals, presence, and size of bubbles, the quantity of dissolved volatiles, and oxygen fugacity, all of which vary both in time and space during emplacement of lava flows. Therefore, a promising approach to more accurately quantify the rheology of lava is to measure it in its natural state via direct field measurements by inserting a viscometer into the lava while it is flowing. Such syn-eruptive, *in-situ* measurements are notoriously difficult to perform due to the lack of appropriate instrumentation and the difficulty of working on or near active lava flows.

In a recent review, Chevrel *et al.* (2019) summarized the few studies that have been published on field lava rheology measurements[21–30]. Two types of instruments have been used; both are derived from methodologies applied in laboratory rheometry: 1) penetrometers, where a penetrating body is pushed into or onto the lava by applying an axial force; this method is commonly used for relatively high viscosity lavas (>$10^{3\text{-}4}$ Pa·s), and 2) rotational viscometers, analogous to the laboratory concentric cylinder method, where a measurement body is inserted into the lava and then rotated. This method is commonly used for low viscosity lavas (<10^4 Pa·s).

These previous studies showed how valuable viscosity measurements in the field are [20,26,28,30]. In particular, such measurements provide precise values of lava viscosity in its natural state that could be implemented into numerical models of actively flowing lava to enable better near-real-time simulation. When calibrated against well-controlled laboratory measurements, results can help to evaluate and quantify the effect of important factors that cannot be reproduced in the laboratory (quantity and size distribution of bubbles and crystals, redox state, quantity of dissolved volatiles).

The device presented here is the continuation of work that started in 2016 when the field viscometer that was created in the 90s by H. Pinkerton from the University of Lancaster[26,28] was recovered, renovated, and tested in an active lava flow on Kilauea in Hawaii[30]. Following these measurements, it became evident that for systematic field measurements to be made, it was necessary to build a new, more mobile, versatile, and lighter viscometer that is equipped with modern data acquisition equipment. Pinkerton's prototype had a total length of the assembled apparatus of 2.7 m, with a weight of about 15 kg (without accounting for the computer and the torque transducer). It required at least 2 people to carry it during measurement and one other to monitor the recording. This proved to be not practical and prevented the use of the device for further investigations [30].

C. Specific requirements

A viscometer designed to be used for measuring the viscosity of flowing lava on volcano flanks involves some specific requirements. The device needs to be portable enough to access remote places. It must be autonomous in energy for a time long enough to ensure several measurements. It must be compact and light enough to be handled and operated by one person so one can easily move around on uneven terrain and approach the active lava stream. The part that is to be immersed must be resistant to the high temperature of around 1200 °C (maximum temperature of currently erupting lava on Earth). The rest of the device does not need to be as heat resistant, as it can be protected by a thermal shield that cuts the radiative heat. Additionally, the device needs to be durable to undergo transport across rough terrains and it must have a security system in place that can easily free the shear vane from the rest of the instrument if cooling lava entraps the immersed vane. The rheometer must be able to cover a large range of rotational speeds and torques to investigate the potential non-Newtonian behavior of lava. Finally, three fundamental parameters must be recorded simultaneously to monitor the measurements. These are i) the rotational speed, ii) the torque imposed by the lava onto the rotating vane, and iii) the temperature at the location of the viscosity measurement. This enables calculation of stress, strain-rate, and ultimately the viscosity of the lava. To explore a large viscosity range, it is helpful if the device can be fitted with a set of shear vanes of various sizes (equivalent diameter and length).

II. INSTRUMENT DESCRIPTION

A. Presentation of the device

The instrument presented here is a rotational viscometer that is based on the principle of Couette's rotating viscometer, as often used in laboratory[31]. At one end there is a shear vane (the part immersed into the molten material) and at the other end a motor drives the vane rotation and a torque sensor, placed between the two, records rotational speed and torque (**Fig. 1**). The shear vane has four blades to 1) enable

easy insertion into the material, 2) avoid slip along the surface of a cylindrical spindle, and 3) achieve the smallest possible spindle volume to minimize cooling of the lava during insertion. The device presented here weighs 12 kg (divided into 3 kg in a backpack and 8 kg in hands) and can be held via two handles, one placed at the front to direct the vane and the other at the back to hold and control the motor. The power supply and data acquisition system are linked via cables and placed in a small backpack. It is very easy to deploy and can be handled and operated by a single person. A thermal shield (such as aluminum foil) can be placed in front of the forward hand to stop radiative heat if necessary (**Fig. 1**).

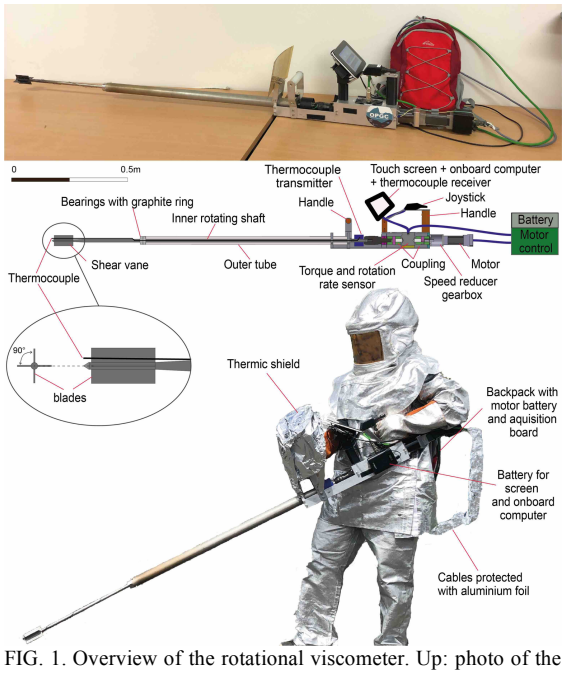

FIG. 1. Overview of the rotational viscometer. Up: photo of the device with the backpack carrying the battery and motor microchip board. Middle: sketch highlighting the main elements (see also exploded view in supplementary information 2). Bottom: operator wearing a fire suit and holding the instrument in the field.

The entire system is controlled by a single board computer Raspberry PI3 that communicates with the various components as described in **Figure 2**. The main components include a motor with its controller, a torque and speed transducer, a temperature sensor, a power supply, and a data acquisition system. The device is controlled via inputs/outputs of the Raspberry PI so that the software can process the information and carry out the corresponding actions (**Fig. 2**). The centralized-on board computer simultaneously records the three fundamental parameters to determine the viscosity of the lava that are the rotation speed, the torque, and the temperature at the shear vane. All the details on the different parts are given in the following sections.

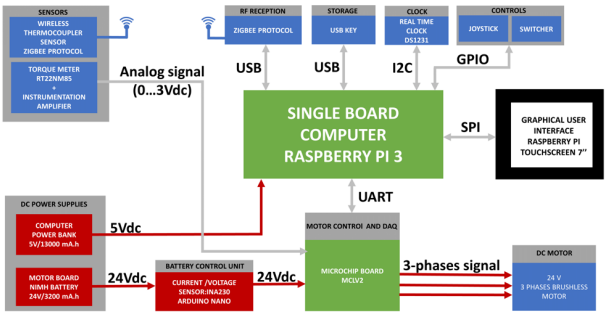

FIG. 2. Flow chart representing the whole system including sensors around the main computer. In blue are the sensors and actuator devices, in green are the development boards (motor and raspberry), in red are the power supplies, and the grey box represents the graphical interface.

B. Hardware description

1. Motor control and data acquisition

The main driver of the viscometer is the motor control system. Despite the use of a precise torque transducer (see next section), the measurements must be done at a steady state (i.e., a constant speed) while minimizing torque oscillations to effectively characterize the viscosity. Another important constraint of the application is to minimize the weight of the instrument. These constraints led to the choice of a Permanent Magnet Synchronous Machine (PMSM). PMSM is more suitable than DC motors or induction motors since the overall weight and volume are significantly reduced for a given output power and they have better efficiency [32]. Moreover, the control choice naturally turned to speed regulation based on Field Oriented Control (FOC) strategy. While six step control is very easy to implement for this motor, FOC has the advantage of controlling the motor currents and thus offers better management of the produced motor torque [33]. This significantly reduces torque oscillations on the motor drive shaft.

The chosen motor is a Hurst DMA0204024B101, equipped with a 250 lines encoder, it has a nominal speed of 3000 RPM and a torque constant of 56mN·m/A. To achieve the desired performance of the application (in terms of rotational speed and torque produced), the motor is equipped with a speed reducer gearbox (IP57 planetary gearbox from McLennan) which reduction factor can be selected depending on the requirement. Here, we either use a factor of 100:1 or 25:1, allowing for a range of rotation per minute (RPM) up to 25 RPM and 100 RPM, respectively. The FOC strategy was implemented using a SAME54 micro-controller with an MLCV2 (Motor Control Low voltage) development board from Microchip Inc. Using MPLAB Device Block for Simulink, the control algorithm was implemented using rapid control prototyping and high-level tools Matlab/Simulink[34]. This hardware performs two main functions which are the motor speed regulation and the digitization of

the analog signal from the torque sensor. Connected to the PC with an RS232 serial communication, it receives speed setpoints from the PC and sends back well-conditioned speed and torque measurements. Note that acquisitions on microcontrollers are obtained from a 12-bit analog-to-digital converter (ADC) that is used to digitize the torque meter signal. The amplified signal from the torque meter is connected to one of the analog channels of the ADC.

2. Torque Sensor

When the motor is running at a constant speed, the viscosity of a material can be obtained from a measure of the torque exerted by the material on the rotating shear vane. This is done with a rotary torque meter. For our purpose, we choose the RT22NM5 from AEP TRANSDUCERS ® that can measure torques from 10 mN·m to 2500 mN·m via a full-scale voltage of 10mV and the output signal of 2mV/V with an accuracy of 0.2% full-scale. This large torque range, which is proportional to the expected stress, ensures that the instrument can measure a wide viscosity range.

The torque sensor consists of a strain gauge bridge that is arranged in an electrical circuit (Wheatstone bridge) and attached to the drive shaft. When a torque is applied, the resulting resistance of the gauge bridge is converted into an electrical signal. This electrical signal is then amplified, digitized, and recorded by the acquisition card (**supplementary material 2**).

For better accuracy, the measurement is scaled (from a 5Vdc power supply to the 3.3V maximum scale of the analog-digital converter (ADC)) knowing that the full-scale voltage of the sensor is 10mV. A differential amplifier is used (INA133) to amplify the signal by 300 and to filter it thanks to a second order low pass Butterworth filter. The precision of the sensor is 0.2% of the full scale or 5mN·m representing a voltage signal after amplification of 6mV. The digitization must be able to detect this minimum value. To do this, the digitization of the signal is carried out by the acquisition card thanks to a 12-bit analog-to-digital converter (supplementary **material 1**).

The torque sensor is factory characterized and the calibration certificate gives a non-linearity error of 0.2%. However, it is necessary to know the transfer function from signal conditioning to digital processing. For this, we checked the linearity of the instrumentation amplifier and the low pass filter and we validated that our processing chain is adapted to the required measurement range.

3. Temperature Sensor

The temperature sensor is a type K thermocouple, insulated with a stainless-steel sheath of 1.5mm diameter and 600mm long, and allows a response time of less than 100 ms. The thermocouple is placed at the level of the shear vane between the blades and inserted into the inner shaft attached to the axis of rotation. The rotating sensor needs a wireless connection to communicate the values. For this, we built an emitter-receiver system with a rotating part of the measurement system made of an electronic digitization card and a processing card. These two cards as well as the battery are integrated into a thermocouple transmitter cylindrical box that is attached to the rotating shaft (**Fig. 1**). The tolerable absolute error of the signal should be a maximum of 1% and this is possible by using a high resolution (24-bit) digitizer and by separating the digitizer and the RF transmission boards (see supplementary **material 1**) which could interfere with the measurement. Data transmission takes place via a wireless link. The transmission of measurements taken on a rotating shaft is frequently done by sliding collectors, but these systems are subject to wear and fouling, which makes precise measurements difficult and may affect the measured torque. The choice fell therefore on a Zigbee system because it provides the fastest hot connection. Energy consumption is optimized because the transmission system goes to sleep after the sending sequence, which lasts about ten milliseconds every 100 ms. This makes it possible to obtain a power consumption of 693µW. An LS14250 type battery provides a battery life of 7 months. The two cards are integrated with a cylindrical box fixed on the rotating shaft. The temperature response has been verified within a furnace using a calibrated thermocouple datalogger.

4. Power sources and acquisition timestamp

The instrument has two main power sources. The onboard computer (Raspberry PI 3) is powered by an external 5Vdc battery with a capacity of 7500mA·h Li-Ion, which allows for one day of autonomous usage. The second is a 24V NiMh battery that powers the motor and the 24-to-5V convertor powering the torque sensor. This type of battery was favored due to its specific energy capacity (W/Kg) which is 30% higher than NiCd batteries and 40% higher than lead batteries. In addition, these NiMh batteries are designed to receive strong transient currents present when the motor is turned on. The INA 230 sensor which measures the battery current and voltage associated with a microcontroller (Arduino nano) controls the state of charge of the battery. An audible signal warns the user of the low battery charge level. The battery can feed the system for up to 8 hours.

The choice of data timestamping falls on a real-time clock (RTC) of the DS3231 type which consumes very little (0.2 mA) compared to a Global Positioning System (20 mA) under 3.3V. The DS3231 is a low-cost real-time clock that incorporates a battery maintaining the time when the main power is off. The RTC can drift by ±2 minutes

per year, but this can be updated by the user in the software.

5. Software and graphical user interface

To visualize the data, we developed a freely accessible software (ViscoMet) in Python that is implemented in the Raspberry PI 3 running under Linux. The PyQt module creates a graphical interface integrating graphs, command buttons, and a toolbar to interact with the viscometer. When starting the software, it launches the initialization sequence and searches for the names of the serial ports to which the motor board and the temperature sensor RF receiver module are connected (**supplementary material 1**). When these steps are valid, the user can execute data acquisition. Otherwise, the user is warned by error messages. The software allows to control the instrument's speed in either manual or automatic mode. In the case of manual mode, the user can set the motor speed by entering the value in a display window or with the joystick button to increase or decrease the speed. In automatic mode, the program executes a speed cycle as defined previously in a text file. A switch allows the motor to be started or stopped at any time by the user. The timing of the acquisition is carried out by a timer which generates an data point every 100 ms. At each point, the data arriving on the serial port is displayed on the digital indicators, and plotted on an updated graph. The data (time, speed, torque, temperature) are saved in a text file on a USB key, ready to be processed later (see details on software architecture in **supplementary material 1**).

6. Design and mechanical conception

In the laboratory, rotational viscometers are vertically placed to ensure alignment and avoid frictional effects that interfere with the torque sensor. For field application, the viscometer is held by hand (**Fig. 1**) and hence will not be vertical but with an angle that will vary depending on the operator's height to the material and the length of the rotating shaft. Each connection between the different parts of the device needs to be aligned with the least friction possible. For this, the torque meter is attached on both sides with a beam coupling. This allows any misalignment to be absorbed. Downstream of the torque sensor, we choose to fix a drill chuck that allows rapid attachment of the rotating shaft. The rotating shaft is a tube (15 mm outer diameter and 2 mm thick wall) to minimize weight and allow the thermocouple wire to be fed through from the vane to the transmitter fixed to the inner tube just before the chuck. This rotating tube is placed inside an outer tube (40 mm outer diameter and 1 mm thick wall) that is fixed to the U-shape base. The rotating shaft is held by the chuck on one side and guided through a bearing assembly containing graphite rings to minimize friction on the high temperature end of the outer tube (**Fig. 1, supplementary material 1**). This helps to maintain alignment at a distance of 1 meter and low-friction rotation of the inner shaft. The shear vane is then screwed to the inner shaft. The shear vane, the inner rotating shaft and the outer tube, and the bearing assemblies are all made using temperature-resistant low carbon stainless steel alloy (BS 321 S20 or Z6CNT18.10). As mentioned by Chevrel *et al.* (2019) this material is resistant both mechanically and to heat. Although its composition (mainly iron) may contaminate the lava, the duration of the measurements is on the order of minutes, preventing significant chemical exchange that could affect the viscosity of the material. Chevrel *et al.* (2019) recommended that the degree of contamination should be investigated in detail in future experiments.

Repeat measurements in high temperature melts (>1000°C) and successive quenching will weaken the stainless-steel shear vane. Thus, the shear vane is designed to be easily exchangeable and could be made of other materials if required.

The rest of the instrument is made of aluminum to minimize the weight. Some parts, like the handles, the thermocouple holder the box for the joystick are made of 3D printed plastic (see exploded view in **supplementary material 1**).

III. DATA PROCESSING AND CALIBRATION

The instrument software is not designed to deliver direct viscosity values, instead, it records the raw data of torque and rotational speed that can then be converted by the user. Data processing must be done after acquisition on an independent system and can follow two different approaches: A) deducing shear stress and shear rate from the measured torque, rotational speed, and vane geometry or B) via calibration of measured torque values to the viscosity of calibration materials. Here we describe both data reduction strategies.

A. Wide gap theory

The theory employed is that of the wide-gap concentric cylinder theory of Couette's rotating viscometer principle[19,28,31,35]. As we use a vane instead of a cylinder, it is assumed that the vane and the trapped fluid between the blades of the vane form a virtual cylinder. The torque is converted into shear stress (τ in Pa) via:

$$\tau = \frac{M}{2\pi h R_i^2} \quad (1)$$

where M is torque (given in mN·m by the instrument), h is vane length and R_i is the radius of the rotating equivalent cylinder (or radius of the vane). The strain rate ($\dot{\gamma}$ in s^{-1}) is calculated from the applied angular velocity of the rotating vane via [10]:

$$\dot{\gamma} = \frac{2\Omega}{n\left(1-\left(\frac{R_i}{R_o}\right)^{2/n}\right)} \quad (2)$$

where R_o is the radius of the container (outer cylinder), n is the flow index (deviation from Newtonian behavior) obtained by calculating the slope of the measured ln(τ) against ln(Ω) with Ω, the angular velocity in rad/s:

$$\Omega = \frac{2\pi\,(RPM)}{60} \qquad (3)$$

where RPM is the number of rotations per minute (motor speed) given by the device.

In equation 2, the radius of the container (R_o) must be known, and $R_i/R_o < 0.97$[36]. However, in the case of measurements of large volume, like in real lava, the shear vane is effectively immersed into an unconstrained medium (i.e., R_o approaches infinity). In that case, Barnes (1989) suggested that the calculation of strain rate (for a range of 0.1 to 10 s^{-1}) can be reduced to:

$$\dot{\gamma} = \frac{2\Omega}{n} \qquad (4)$$

This means that the rotational viscometer can be used in any volume (sufficiently large for the shear vane to be inserted).

To assess the material's rheological behavior (Newtonian or not), the stress can be plotted against the strain rate to produce flow curves[37].

B. Calibration using certified viscosity standards

For the measurements in lava presented later in the manuscript, the instrument was calibrated using two certified viscosity reference standards. One is the N190000 from Cannon Instrument Company® that covers a high viscosity range from 800 Pa·s at 20°C to 32 Pa·s at 60°C and the other is the N15000 from Brant Industry® with a lower viscosity ranging from 62 Pa·s at 20°C to 5 Pa·s at 50°C. To perform the calibrations, 1L of viscosity standard was poured into a cylindrical glass beaker of 10 cm diameter and 15 cm depth and we used a shear vane of 80 mm length and 25 mm radius (SV 80/25). Before each calibration run, the standard oil was either placed in an oven at the desired temperature overnight to allow temperature equilibration and removal of all air bubbles or simply left at room temperature. During the experiment, the container was placed into a water bath at the desired temperature to maintain constant thermal conditions.

The N190000 experiments were performed at four different temperatures (22, 25, 40, and 60 °C), while the N15000 experiment was performed at two temperatures (23 and 34 °C). Experiments were conducted over a wide range of strain rates with velocities from 0.5 to 25 RPM for the N190000 and up to 100 RPM for the N15000. Given the geometry of the cylindrical container and the shear vane the rotational speed range corresponds to strain rates ranging from 0.1 s^{-1} at 0.5 RPM to 27.9 s^{-1} at 100 RPM. With the current torque sensor (max torque: 2500 mN·m) and the shear vane geometry, the maximum stress is calculated to be 7800 Pa. In most experiments, measurements were performed under increasing rotational velocity steps followed by decreasing velocity steps (**Fig. 3**). Note that we observed slight viscous heating of the fluid (0.5°C, Fig. 3b) during the measurements.

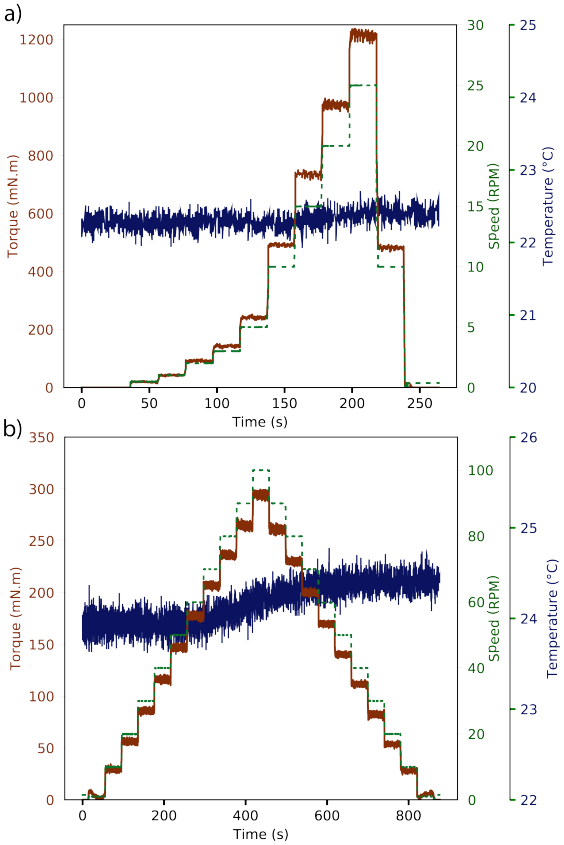

FIG 3: Example of raw data acquisition using the shear vane 80mm long and 25mm in radius in the viscosity standards: a) N190000 at 22.3°C and b) N15000 at 24.1 °C. Torque (dark red), rotational speed (green dash), and temperature (blue) are simultaneously displayed.

To test the instrument and for calibration purposes, we extracted the flow index n from the relationship ln(τ) - ln(Ω). This is to test that, over the applied rotational velocity range, the recorded torque was indeed proportional to the shear rate, corroborating the Newtonian behavior of the standard oil. We found that torque values below 10 mN·m (equivalent to stress values below 30 Pa for the selected geometry) deviated from the linear trend, indicating that internal effects such as bearing friction started to affect the measurement quality (**Fig. 4**). Additionally, stress accuracy due to standard deviation on the torque measurement was higher than 10% for torque lower than 20 mN·m but is systematically lower than 5% for torques higher than 30 mN·m. Thus, measurements below 10 mN·m were discarded and the results indicated a flow index n = 1±0.05 for the two standard oils under all explored temperatures, validating the capabilities of the viscometer (**Fig. 4**).

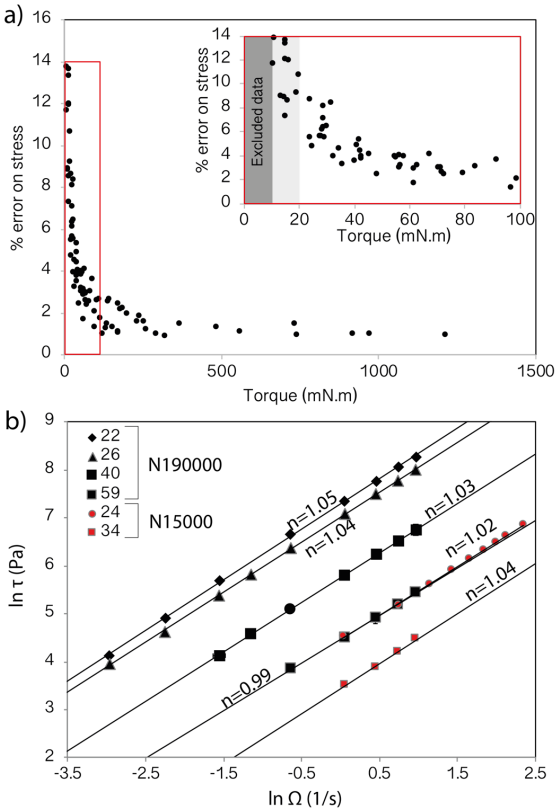

FIG 4. Data processing using a shear vane that is 80mm long and 25 mm radius. a) torque values lower than 10 mN·m are excluded and values lower than 20 mN·m have errors as large as 10 %. b) Estimation of the flow index *n*. Experiments at 22°C for N190000 and 24°C for N15000 are the ones presented in Figure 6. Error on torque values and propagated to stress values are lower than symbols.

Knowing the limit of the instrumentation (i.e. no value lower than 10mN·m are used and linear response of the torque sensor within increasing rotation viscosity), and to extract accurate viscosity, we follow a calibration procedure that is commonly applied also in laboratory measurements[4,12,18,38,39]. For this, the certified viscosity values provided for the standard oils were used to define an exponential relationship between viscosity and temperature. These are: $\eta = 3703\ e^{-0.08T}$ (R^2=0.99) for N190000 and $\eta = 284\ e^{-0.08T}$ (R^2=0.99) for N15000. Since the viscosity standard oils are Newtonian, stress increases proportionally with strain rate according to a factor equal to viscosity. Hence for a given temperature (i.e, a given viscosity using the above-mentioned equations), we calculate a torque–viscosity relationship by finding the calibration coefficient α for a given rotation rate (RPM; Table 1) and defined as:

$$\eta = \alpha M \quad (5)$$

Note that the intercept of this linear fit is defined at 0 although it is not always exactly the case in the measurements due to frictional effects within the instrument at low rotation rate and torque (i.e. there is a minimum measurable viscosity). The R^2 of these linear fits is larger than 0.9 for all velocities except for 0.5 RPM.

RPM	α	R^2
0.5	31.01	0.825
1	14.81	0.999
2	6.92	0.996
3	4.42	0.997
5	2.61	0.999
10	1.28	0.999
15	0.85	0.999
20	0.64	0.998
25	0.51	0.999
40	0.38	0.933
60	0.25	0.924
80	0.18	0.948
100	0.14	0.955

TABLE 1. Calibration coefficient for each applied rotational velocity (RPM) and corresponding R^2 value.

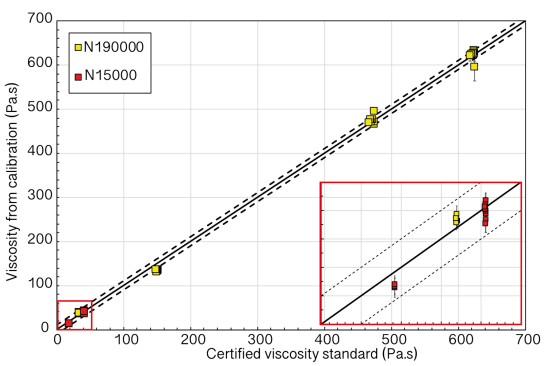

FIG 5: Certified standard viscosity for a given temperature (using the standard oil N190000 and N15000) versus measured viscosity with calibration using the shear vane than 80mm long and 25 mm radius. The solid line gives the 1:1 relationship and the dashed lines delimit an interval of ±10 Pa·s.

Following this calibration, viscosity is obtained for any given rotational velocity (i.e. a given strain-rate) by calculating the average torque recorded over the period where the rotational velocity is constant. Applying the calibration (**Table 1**), we extracted the viscosity from our measurements and compare them to the viscosity of the certified standard (**Fig. 5**). Results indicate that the rotational viscometer reproduces the viscosity values within 10 Pa·s accuracy for a large viscosity range up to 650 Pa·s. This is considerably better in comparison to the previous viscometer that had a confidence interval of ± 50 Pa·s[30]. Note that the calibration of the device was validated through measurements at varying immersion angles and results show that deviation in measured torque between the vertical calibration and angled hand-held measurements is smaller than measurement noise.

IV. MEASUREMENTS IN LAVA

To further validate the use of the field viscometer and evaluate potential unwanted effects that could arise from the extreme conditions when measuring

in active lava and when operating by hand, we performed high temperature tests at the geohazards field station of the University at Buffalo. Large-scale experiments were carried out within a furnace with a capacity of approx. 25 L lava volume at temperatures ranging from 1100°C to 1350 °C. For these tests, the operator is located above the furnace and holds the viscometer which is then manually immersed in the molten lava (**Fig. 6**). The quantity of lava, the size of the container, and the angle at which the viscometer is positioned are chosen to ensure the shear vane is fully immersed in the lava (**Fig. 6b**).

FIG 6: Measurements in a large-scale furnace. a) general view; b) view from the operator angle.

We performed tests using two different re-melted basaltic lavas, one from Chengwatana, Wisconsin (same material as used in[40,41]) and another basanite lava from the Balcones Igneous Province in Texas[42,43]. Six experiment runs were performed, three for each lava type. Each run lasted between 1 to 2 minutes. Akin to the calibration procedure described above, we followed a speed step protocol, where the rotational velocity increased in steps of 20 RPM from 20 to 100 RPM and then decreased following the same ramp.

As to be expected when moving from a controlled laboratory setting with a fixed stand to a high temperature environment and manual operation, the data recorded in the lava measurements are not as smooth as the calibration measurements presented in **Fig. 3** (see **supplementary material 2**). There are two main factors to be considered: First, the movement of the operator that might lead to the deviation of the immersed shear vane from the center of the furnace toward the wall may have an impact on the data (increasing wall effects). Second, the entrainment of cooler material from the crust and/or textural heterogeneities within the melt that can affect the measured torque value. The temperature measurement is very responsive to changes, and we can observe variations during the experiment that indicate the presence of cooler material within the melt (see **supplementary material 2**). Other heterogeneities include temperature gradients from the sides, bottom, and top of the crucible, as well as intermittent chunks of cooled crust that remain immersed in the melts and, at times, interact with the spindle during rotation – causing spikes in the measured torque. One of the fundamental strengths of the device presented here is that all relevant data are recorded simultaneously. This enables the user to scrutinize every part of the measurements and make informed decisions on which data are an accurate representation of the viscous properties of the material and which data are to be discarded because they are affected by external factors. We find that instabilities in the torque readings can frequently be directly correlated to the entrainment of cooler (more viscous to rigid) material from the crusted surface.

We evaluate the data from these lava measurements and only selected the steps for which the torque and temperature was stable. This is done following the approach detailed in **supplementary material 2**, where we present the data validation procedure together with examples of how to identify both valid and invalid measurements. During this validation step, the raw data is filtered, and only stable reading portions are considered. To the data that passed the quality assessment step, we applied the calibration (**Table 1**) and extracted the viscosity from our measurements at each velocity step. These data are plotted in **Figure 7.**

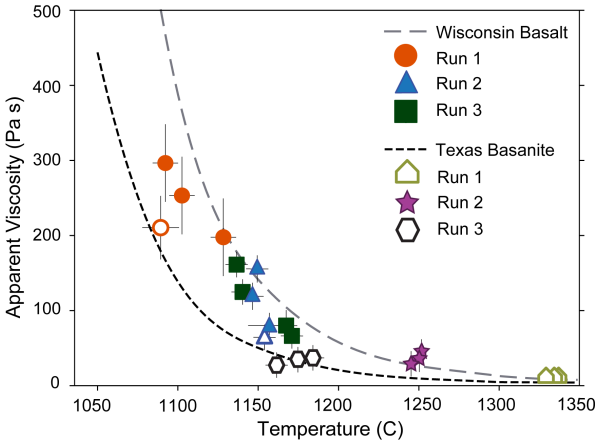

FIG 7: Viscosity of the re-melted basaltic lava from Chengwatana, Wisconsin, and basanite lava from the Balcones Igneous Province, Texas. Dashed lines represent the theoretical temperature-dependent viscosity curves calculated for the bulk rock composition via an empirical model[6]. Data from three separate runs of each rock type are plotted over the model curves. Each marker represents the mean viscosity from a specific speed step in the measurement. Solid-filled markers show data calculated from steps with relatively stable torque and temperature readings, and open-filled markers show data calculated from steps with stable torque but unstable temperature readings. When the individual step standard deviations are larger

than the size of the marker, 2σ bars are shown. The error bars represent the viscosity variation due to torque noise and temperature range during the measurement time calculated over 270 to 488 data points depending on the experiment (see supplementary material 2).

After each measurement, the shear vane was extracted from the lava and quickly immersed in water to quench the material for subsequent textural and compositional analyses. Bulk rock major element analysis of the sample was carried out with inductively coupled plasma–atomic emission spectroscopy at the Laboratoire Magmas et Volcans (LMV, Université Clermont-Auvergne, France). The viscosity of each rock type (i.e., Wisconsin Basalt and Texas Basanite) was modelled at the measured average temperature and using the bulk rock chemical composition following an empirical model[6].

Results indicate that the measured viscosity agrees with the theoretical viscosity of two different rock compositions (**7**). The Texas basanite sample is extremely low in viscosity (< 40 Pa·s), and at high temperatures, it represents the lower measurement limit of the device based on the torque sensor capabilities (see further discussion below). Despite the low viscosity of the basanite, the measured viscosities spanning ~200˚ C (1150-1350˚ C) is consistent with the empirical model curve. Likewise, the measured viscosity of the Wisconsin Basalt, which has a slightly higher viscosity than the basanite, fits the empirical model curve over ~80˚C (1100-1180˚C). A detailed data validation procedure can be found in **supplementary material 2**.

The instruments resisted the high temperatures of the lava measurement very well. The steel spindles that were immersed in lava up to 1350˚ C incurred no deformation and could be reused in subsequent measurements. Additionally, the thermocouples, which were also immersed in the high temperature lava were not damaged, and all other electronic components (i.e., torque sensors, Raspberry Pi, etc.) were adequately shielded from the high heat and suffered no damage or failure of efficacy.

V. PERSPECTIVES

A. Advantages and limitations of the instrument

The field rotational viscometer has been calibrated to viscosity ranging from 10 to 650 Pa·s. It is tried and tested to measure large volumes of high temperature material, such as lava (<1350°C). One of the main advantages of this instrument, thanks in part to improved wireless transmission and an acquisition speed of 100 ms, is near real time synchronized measurements of temperature, torque, and rotational velocity, enabling detailed data validation post measurement. This was not the case in previous versions of field viscometers[30]. Although this field rotational viscometer has been designed for volcanology, it can be operated in different contexts such as industrial melt production processes.

In its current state, the viscometer is limited to a viscosity higher than 10 Pa·s. Tests at lower viscosity (e.g. using the N15000 at 48°C and Texas lava at 1350°C) showed that the instrument retrieved a viscosity that falls within 10 Pa·s (**5b**) but with a deviation from the calibrated viscosity of up to 40 %. This large deviation is mainly due to the torque sensor accuracy (5 mN·m) and friction within the mechanical assembly that limits accurate measurements below 10 Pa·s. Given the current maximum torque that the torque sensor can measure (up to 2500 mN·m.), the minimum speed (1 RPM), the maximum viscosity that could potentially be measured is as high as 3×10^4 Pa·s using the given vane geometry of 80mm long with a radius of 25 mm.

B. Future application to lava flows

The use of the viscometer to measure the viscosity of lava flows is challenged by the difficulty of approaching active lava on volcanoes. Working at an active volcanic site is not an easy task and required great knowledge of the environment. However, in the case of basaltic lava effusion, which typically has viscosities ranging from 10^1-10^4 Pa·s and can usually be approached, measurements are possible as already done by previous studies[20,28–30].

To deploy the instrument on an active lava flow, we have several recommendations. Approaching a lava flow has to be made up-wind to avoid being exposed to the heated air and volcanic gasses blown from the lava. To perform the measurement, the operator needs to be as close as 1 m meter (the length of the rotating shaft and vane) to the active lava. Due to the proximity to the lava, the operator must wear a complete fire suit (clothes + helmet) to be protected from the radiative heat emitted by the lava (**Fig. 1**). All exposed skin will be burned by the radiation if not well covered. The measurement must last until the torque reading is stable at a given rotational velocity but cannot be longer than a couple of minutes because of the extreme heat inflicted on the operator, despite the fire suit. Indeed, it is most likely that the human operator will no longer be able to withstand the heat before any part of the instrument is damaged.

When inserting the shear vane into hot material, the temperature contrast between the cold metal shear vane and the hot material may form a cooler layer at the contact with the metal. Care should be taken that the thermocouple tip is sticking out of the shear vane (**Fig. 1**) to avoid becoming entrapped into this cooler crust and hence isolating it from the molten material (resulting in inaccurate temperature readings). To reduce the effects of crust formation (that may disturb both torque and temperature measurement),

the shear vane, therefore, must be pre-heated[20]. Pre-heating can simply be done by exposing the vane to the lava (a few centimeters above the radiating lava over a couple of minutes has proven to be sufficient), before immersion.

To insert the viscometer into the lava and obtain a stable reading, the operator must stay still over the time of the measurement. For this, standing on the stable ground must be ensured. Care should be taken to keep the vane location stable within the lava without touching the cooler flow base or sides. The shear vane must be completely inserted within the fluid interior emerging through breaches in the crust or at the breaking point of pāhoehoe lobes, where little-to-no crust is present and not in the cooler visco-elastic crust[20].

Once the measurement is done, the shear vane should be quickly withdrawn from the lava and quenched in a bucket of water to ensure the sample best represents the lava during measurement. This will freeze-in the lava's physico-chemical and textural properties before any modifications due to slower cooling (microcrsystallization, element diffusivity, post-sampling vesiculation, and expansion)[20]. Such a sampling method ensures retrieval of the proportion of phases, glass composition, and redox state[20].

The present viscometer can measure the viscosity of fully molten lava, as well as multiphase suspensions (crystal and bubble bearing lava suspension). Applications to active lavas should include measurement at various locations and times along the same lava flow or flow field. This would allow us to fully describe the lava rheological evolution downflow as cooling and degassing occur. Results could then be used to develop, run or calibrate numerical models that lack field-validated values of lava viscosity. The success of such *in-situ* field measurements will greatly improve our understanding of evolving lava viscosity as a function of cooling rate, degassing, and crystallization, which has been so far limited due to the lack of adequate instrumentation[20]. With this new rotational viscometer, this is now achievable and it is therefore now time to deploy it on active volcanic systems.

V. CONCLUSION

We present a new field rotational viscometer that is completely transportable, does not require any external energy source, and can be handled by a single person. The field rotational viscometer simultaneously acquires and displays the three fundamental parameters in real time to determine the viscosity of a medium: i.e. rotation speed, torque, and temperature. Viscosity measurements can be performed at very high temperatures (up to 1350°C) and over a wide range of stress (30 - 10^3 Pa), strain rate (0.1 - 28 s^{-1}), and viscosity (10 – 10^4 Pa·s), depending on the vane geometry. The rotation speed of the shear vane can be varied manually or pre-programed. The instrument is versatile and key functional components can be changed to adapt to the environment (any shape and size of shear vanes can be used; speed reducer gearbox and torque sensor can also be changed for different purposes). The instrument has been calibrated against certified viscosity standards over a viscosity range of 10 to 650 Pa·s and tested in the lava at up to 1350°C. This unique field rotational viscometer is now ready to be used in real conditions either in lava flows on volcanoes or in industry.

VI. SUPPLEMENTARY MATERIAL

Supplementary material 1: the exploded view of the rotational viscometer, the conditioning and processing of the torque signal, the flow chart for temperature transmission system and the software class diagram.

Supplementary material 2: A detailed description of the data validation procedure.

VII. AUTHOR CONTRIBUTIONS

MO Chevrel conceptualized and managed the project, performed all the tests and calibrations, and led the redaction of the article. T Latchimy was in charge of the acquisition chain, electronics, and software. L Batier participated in the mechanical conception and was in charge of the CAO. R Delpoux was in charge of the motor setup and acquisition. S. Kolzenburg, and M. Harris performed the lava measurements at the UB facility. All authors contributed to the writing of the article.

VIII. ACKNOLEDGEMENTS

Special acknowledgement to Harry Pinkerton, who built the first portable field viscometer and allowed us to use his last version and improve it. We acknowledge all the people who participated in the project in particular Christelle Rossin and Claude Berlie-Caillat as well as various colleagues who were very supportive. We greatly thank Ingo Sonder for operating the UB geohazards field station facility and Jason Travis Parsons who helped with lava measurements.

IX. FUNDING

This project was funded by "Actions Incitatives de l'Observatoire Physique du Globe de Clermont" 2017 and by Chèque Recherche Innovation Hub Innovergne 2021 from I-site, Clermont-Ferrand (PRHI-3.2-CRI200506-CHEVREL). The project started with the Auvergne fellowship attributed to MO Chevrel 2015-2017 and beneficiated from the support of ANR LAVA project (Program: DS0902 2016; Project: ANR-16 CE39-0009). Funding for the high temperature tests at UB was provided by the UB geohazards center and an NSF EAR RAPID grant (Award Number: 2241489). This project also received support from the Institut de Recherche pour

le Développement (IRD) and the French Gouvernment Laboratory of Excellence initiative No. ANR-10-LABX-0006. This is a Laboratory of Excellence ClerVolc contribution n°619.

AUTHOR DECLARATIONS

Conflict of Interest

The authors have no conflicts to disclose.

Author contributions

MO Chevrel conceptualized and managed the project, performed all the tests and calibrations, and led the redaction of the article. T Latchimy was in charge of the acquisition chain, electronics, and software. L Batier participated in the mechanical conception and was in charge of the CAO. R Delpoux was in charge of the motor setup and acquisition. S. Kolzenburg, and M. Harris performed the lava measurements at the UB facility. All authors contributed to the writing of the article.

DATA AVAILABILITY

All data that support the findings of this study are available upon request to the corresponding author. The software is openly available at https://github.com/ThierryLat/ViscoMeter.

REFERENCES

1. Smith, J. V. Textural evidence for dilatant (shear thickening) rheology of magma at high crystal concentrations. *J. Volcanol. Geotherm. Res.* **99**, 1–7 (2000).
2. Dingwell, D. B. Volcanic Dilemma Flow or Blow. *Science (80-.).* **273**, 1054–1055 (1996).
3. Dingwell, D. B. Transport Properties of Magmas Diffusion and Rheology. *Elements* **2**, 281–286 (2006).
4. Kolzenburg, S., Chevrel, M. O. & Dingwell, D. B. Magma suspension rheology. *Rev. Mineral. Geochemitry* **87**, 639–720 (2022).
5. Harris, A. J. L. & Rowland, S. K. Lava flows and rheology. *Encycl. Volcanoes, 2nd Ed. Eds Sigurdsson H, Hought. B, McNutt SR, Rymer H, Styx J* (2015).
6. Giordano, D., Russell, J. K. & Dingwell, D. B. Viscosity of magmatic liquids: A model. *Earth Planet. Sci. Lett.* **271**, 123–134 (2008).
7. Mader, H. M., Llewellin, E. W. & Mueller, S. P. The rheology of two-phase magmas: A review and analysis. *Bull. Volcanol.* **257**, 135–158 (2013).
8. Marsh, B. D. On the Crystallinity, Probability of Occurrence, and Rheology of Lava and Magma. *Contrib. Miner. Pet.* **78**, 85–98 (1981).
9. Ryerson, F. J., Weed, H. C. & Piwinskii, A. J. Rheology of subliquidus magmas, 1. Picritic compositions. *J. Geophys. Res.* **v. 93**, 3421–3436 (1988).
10. Stein, D. J. & Spera, F. J. New high-temperature rotational rheometer for silicate melts, magmatic suspensions, and emulsions. *Rev. Sci. Instrum.* **69**, 3398–3402 (1998).
11. Dingwell, D. B. Viscosity-temperature relationships in the system Na2Si2O5-Na4Al2O5. *Geochim. Cosmochim. Acta* **50**, 1261–1265 (1986).
12. Kolzenburg, S., Giordano, D., Cimarelli, S. & Dingwell, D. B. In situ thermal characterization of cooling/crystallizing lavas during rheology measurements and implications for lava flow emplacement. *Geochim. Cosmochim. Acta* **195**, 244–258 (2016).
13. Harris, A. J. L., Favalli, M., Wright, R. & Garbeil, H. Hazard assessment at Mount Etna using a hybrid lava flow inundation model and satellite-based land classification. *Nat. Hazards* **58**, 1001–1027 (2011).
14. Cordonnier, B., Lev, E. & Garel, F. Benchmarking lava-flow models. *Detect. Model. Responding to Effusive Eruptions. Eds, Harris AJL, Groeve T, Garel F Carn SA, Geol. Soc. London, Spec. Publ.* **426**, (2015).
15. Chevrel, M. O., Harris, A. J. L., Peltier, A., Villeneuve, N., Coppola, D., Gouhier, M. & Drenne, S. Volcanic crisis management supported by near real time lava flow hazard assessment at Piton de la Fournaise, La Réunion. *Volcanica* **5**, 313–334 (2022).
16. Ganci, G., Vicari, A., Cappello, A. & Del Negro, C. An emergent strategy for volcano hazard assessment: From thermal satellite monitoring to lava flow modeling. *Remote Sens. Environ.* **119**, 197–207 (2012).
17. Dietterich, H. R., Lev, E., Chen, J., Richardson, J. A. & Cashman, K. V. Benchmarking computational fluid dynamics models of lava flow simulation for hazard assessment, forecasting, and risk management. *J. Appl. Volcanol.* **6**, (2017).
18. Dingwell, D. B. Viscosity-temperature relationships in the system Na2Si2O5-Na4Al2O5. *Geochim. Cosmochim. Acta* **50**, 1261–1265 (1986).
19. Spera, F. J., Borgia, A., Strimple, J. & Feigenson, M. Rheology of melts and magmatic suspensions I. Design and calibration of a concentric cylinder viscometer with application to rhyolitic magma. *J. Geophys. Res.* **93**, 10273–10294 (1988).

20. Chevrel, M. O., Pinkerton, H. & Harris, A. J. L. Measuring the viscosity of lava in the field: A review. *Earth-Science Rev.* **196**, (2019).
21. Einarsson, T. The flowing lava. Studies of its main physical and chemical properties. in *The eruption of Hekla 1947-1948* vol. IV 1–70 (Soc Scientiarum Islandica, Reykjavik, 1949).
22. Shaw, H. R., Wright, T. L., Peck, D. L. & Okamura, R. The Viscosity of Basaltic Magma: An analysis of Field Measurements in Makaopuhi Lava Lake, Hawaii. *Am. J. Sci.* **266**, 225–264 (1968).
23. Gauthier, F. Field and laboratory studies of the rheology of Mount Etna lava. *Philos. Trans. R. Soc. London A Math. Phys. Eng. Sci.* **274**, 83–98 (1973).
24. Pinkerton, H. & Sparks, R. S. J. Field measurements of the rheology of lava. *Nature* **276**, 383–385 (1978).
25. Panov, V. K., Slezin, Y. B. & Storcheus, A. V. Mechanical properties of lavas extruded in the 1983 Predskazannyi eruption (Klyuchevskoy volcano). *Volcanol. Seismol.* **7**, 25–37 (1988).
26. Pinkerton, H., Herd, R. A., Kent, R. M. & Wilson, L. Field measurements of the rheological properties of basaltic lavas. *Lunar Planet. Sci.* **XXVI**, 1127–1128 (1995).
27. Pinkerton, H., Norton, G. E., Dawson, J. B. & Pyle, D. M. Field observations and measurements of the physical properties of Oldoinyo Lengai alkali carbonatite lavas, November 1988. in *IAVCEI Proceedings in Volcanology 4. Carbonatite volcanism of Oldoinyo Lengai - petrogenesis of natrocarbonatite.* (eds. Bell, K. & Keller, J.) 23–36 (Springer-Verlag, Berlin, 1995).
28. Pinkerton, H. & Norton, G. Rheological properties of basaltic lavas at sub-liquidus temperatures: laboratory and field measurements on lavas from Mount Etna. *J. Volcanol. Geotherm. Res.* **68**, 307–323 (1995).
29. Belousov, A. & Belousova, M. Dynamics and viscosity of ʻaʻā and pāhoehoe lava flows of the 2012-2013 eruption of Tolbachik volcano, Kamchatka (Russia). *Bull. Volcanol.* **80**, (2018).
30. Chevrel, M. O., Harris, A. J. L., James, M. R., Calabrò, L., Gurioli, L. & Pinkerton, H. The viscosity of pāhoehoe lava: In situ syn-eruptive measurements from Kilauea, Hawaii. *Earth Planet. Sci. Lett.* **493**, 161–171 (2018).
31. Borgia, A. & Spera, F. J. Error analysis for reducing noisy wide-gap concentric cylinder rheometric data for nonlinear fluids: Theory and applications. *J. Rheol. (N. Y. N. Y).* **34**, 117–136 (1990).
32. Glumineau, A. & De Leon Morales, J. Sensorless AC Electric Motor Control. in (2015). doi:https://doi.org/10.1007/978-3-319-14586-0.
33. Blaschke, F. The principle of field orientation applied to the new transvector closed loop system for rotating field machines. *Siemens Rev.* **34**, 217–220 (1972).
34. Delpoux, R., Kerhuel, L. & Léchappé, V. On Chip Rapid Control Prototyping for DC Motor. *J3eA J. Sur l'enseignement Des Sci. Technol. l'information Des Systèmes* (2021).
35. Stein, D. J. & Spera, F. J. Rheology and microstructure of magmatic emulsions: Theory and experiments. *J. Volcanol. Geotherm. Res.* **49**, 157–174 (1992).
36. Barnes, H. A. *An Introduction to Rheology*. *Rheology series 3* (U.S. and Canada, Elsevier Science, 1989).
37. Lenk, R. S. A Generalized Flow Theory. *J. Appl. Polym. Sci.* **11**, 1033–1042 (1967).
38. Chevrel, M. O., Cimarelli, C., DeBiasi, L., Hanson, J. B., Lavallée, Y., Arzilli, F. & Dingwell, D. B. Viscosity measurements of crystallizing andesite from Tungurahua volcano (Ecuador). *Geochemistry, Geophys. Geosystems* **16**, 870–889 (2015).
39. Vona, A. & Romano, C. The effects of undercooling and deformation rates on the crystallization kinetics of Stromboli and Etna basalts. *Contrib. to Mineral. Petrol.* **166**, 491–509 (2013).
40. McClinton, J. T. & White, S. M. Emplacement of submarine lava flow fields: A geomorphological model from the Nin~os eruption at the Gal?apagos Spreading Center. *Geochemistry Geophys. Geosystems* **16**, 267–300 (2015).
41. Lev, E., Spiegelman, M., Wysocki, R. J. & Karson, J. A. Investigating lava flow rheology using video analysis and numerical flow models. **248**, 62–73 (2012).
42. Sonder, I., Harp, A. G., Graettinger, A. H., Moitra, P., Valentine, G. A., Büttner, R. & Zimanowski, B. Meter-Scale Experiments on Magma-Water Interaction. *J. Geophys. Res. Solid Earth* **123**, 10,510-597,615 (2018).
43. Griffin, W. R., Foland, K. A., Stern, R. J. & Leybourne, M. I. Geochronology of Bimodal Alkaline Volcanism in the Balcones Igneous Province, Texas: Implications for Cretaceous Intraplate Magmatism in the Northern Gulf of Mexico Magmatic Zone. *J. Geol.* **118**, 1–21 (2010).

Chevrel MO, Latchimy T, Batier L, Delpoux R, Harris M, Kolzenburg S. A new portable field rotational viscometer for high-temperature melts. Rev Sci Instrum. 2023 Oct 1;94(10):105116. doi: 10.1063/5.0160247.

SUPPLEMENTARY MATERIAL 1

for

A new portable field rotational viscometer for high-temperature melts

M. O. Chevrel[1,2,3,a)], T. Latchimy[1], L. Batier[4], R. Delpoux[5], M. Harris[6], S. Kolzenburg[6]

[1]*Université Clermont Auvergne, CNRS, IRD, OPGC, Laboratoire Magmas et Volcans, 63000 Clermont-Ferrand, France.*
[2]*Université Paris Cité, Institut de physique du globe de Paris, CNRS, 75005 Paris, France*
[3]*Observatoire volcanologique du Piton de la Fournaise, Institut de physique du globe de Paris, 97418 La Plaine des Cafres, France*
[4]*Université Clermont Auvergne, Polytech Clermont, 63000 Clermont-Ferrand, France.*
[5]*Univ Lyon, INSA Lyon, Université Claude Bernard Lyon 1, Ecole Centrale de Lyon, CNRS, Ampère, UMR5005, 69621 Villeurbanne, France*
[6]*Department of Geology University at Buffalo, 126 Cooke Hall Buffalo, NY 14260-4130, USA*

a) corresponding author: oryaelle.chevrel@ird.fr

This Supplementary Material contains four figures:

1) Figure S1: An exploded view of the rotational viscometer
2) Figure S2: Conditioning and processing of the torque signal
3) Figure S3: Flow chart representing the temperature measurement transmission system
4) Figure S4: Software class diagram describing the various functions

Figure S1: An exploded view of the rotational viscometer

Number	Description	Material	Quantities
1	U-shape base bottom	Aluminium	1
2	U-shape top	Aluminium	
3	Holder external tube to base	Aluminium	2
4	Holder ball bearing to base	Aluminium	1
5	Cap to holder ball bearing	Aluminium	2
6	Holder motor to base	Aluminium	1
7	Motor+reductor		1
8	Coupling	Aluminium	2
9	Torque sensor		
10	Holder torque sensor to base	Aluminium	1
11	Cap for inner ring for ball bearing	Aluminium	1
12	Inner ring for ball bearing	Aluminium	1
13	Ball bearing	Stainless steel	2
14	Drill chuck	Metal	1
15	Box of thermocouple emiter	Plastic	1
16	Connector shaft-chuck	Stainless steel	1
17	Rotating shaft	Stainless steel	
18	Connector shaft-shear vane	Stainless steel	2
19	Shear vane	Stainless steel	1
20	Cap graphite ring	Stainless steel	1
21	Ring	Graffite	1
22	Holder grafite ring	Stainless steel	1
23	Outer tube	Stainless steel	1
24	Handle	Plastic	1
25	Handle	Plastic	1
26	Top handle	Aluminium	1
27	Ion/off button	Plastic	1
28	Joystick on/off	Plastic	2
29	box joystick	Plastic	1
30	box joystick	Plastic	1
31	touch screen holder	Plastic	1
32	Touch screen with Raspberry Pi		1
33	Handle holder	Aluminium	2
34	Handle	Plastic	1
35	Frame holder to thermal shield	Aluminium	1
36	Thermic shield	Aluminium	1

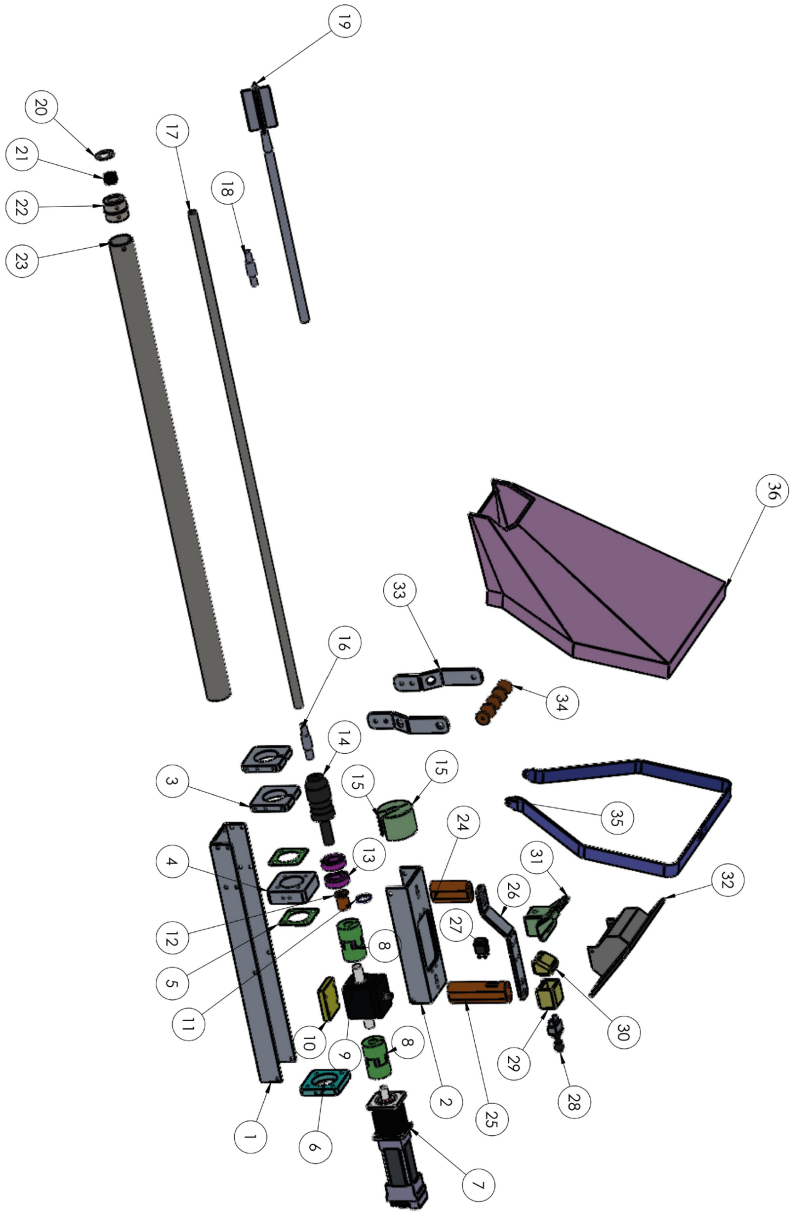

Figure S2: Conditioning and processing of the torque signal

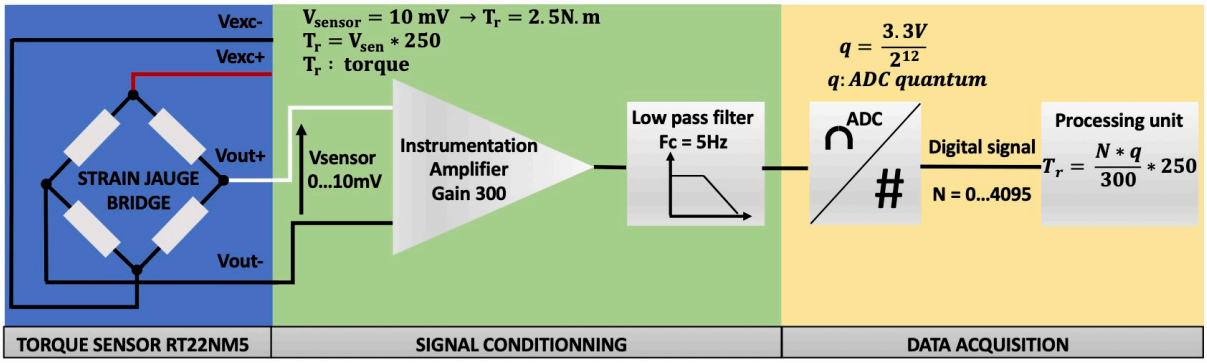

Figure S3: Flow chart representing the temperature measurement transmission system

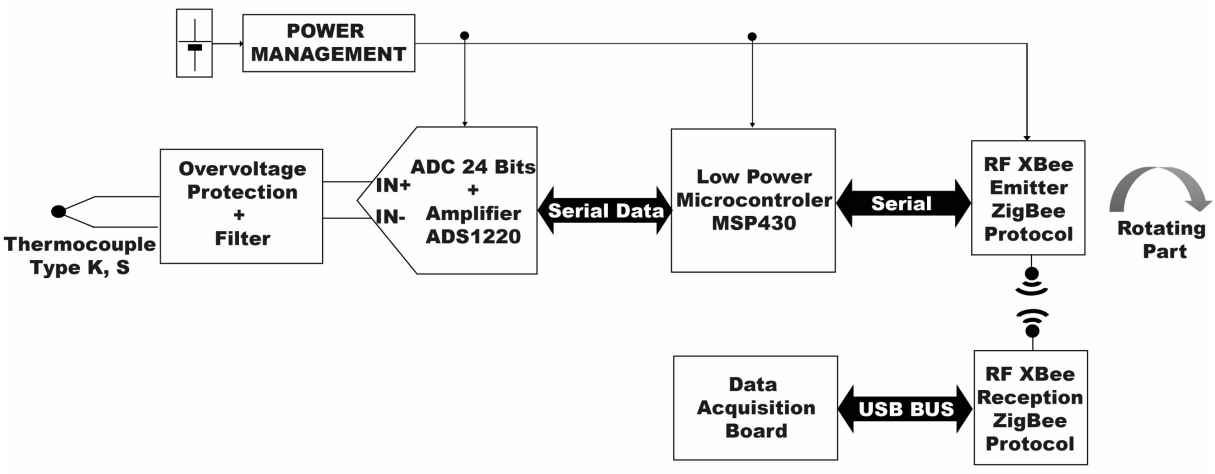

Chevrel MO, Latchimy T, Batier L, Delpoux R, Harris M, Kolzenburg S. A new portable field rotational viscometer for high-temperature melts. Rev Sci Instrum. 2023 Oct 1;94(10):105116. doi: 10.1063/5.0160247.

SUPPLEMENTARY MATERIAL 2

for

A new portable field rotational viscometer for high-temperature melts

M. O. Chevrel[1,2,3,a)], T. Latchimy[1], L. Batier[4], R. Delpoux[5], M. Harris[6], S. Kolzenburg[6]

[1]*Université Clermont Auvergne, CNRS, IRD, OPGC, Laboratoire Magmas et Volcans, 63000 Clermont-Ferrand, France.*
[2]*Université Paris Cité, Institut de physique du globe de Paris, CNRS, 75005 Paris, France*
[3]*Observatoire volcanologique du Piton de la Fournaise, Institut de physique du globe de Paris, 97418 La Plaine des Cafres, France*
[4]*Université Clermont Auvergne, Polytech Clermont, 63000 Clermont-Ferrand, France.*
[5]*Univ Lyon, INSA Lyon, Université Claude Bernard Lyon 1, Ecole Centrale de Lyon, CNRS, Ampère, UMR5005, 69621 Villeurbanne, France*
[6]*Department of Geology University at Buffalo, 126 Cooke Hall Buffalo, NY 14260-4130, USA*

a) corresponding author: oryaelle.chevrel@ird.fr

This supplementary material contains the data selection and validation procedure for high-temperature measurements including explanation and a figure.

Data Selection and Validation Procedure for High-Temperature Measurements**:**

We performed high temperature tests at the geohazards field station of the University at Buffalo. Large-scale experiments were carried out within a furnace with a capacity of about 25 L lava volume at temperatures ranging from 1100°C to 1350 °C. Measurements were not as smooth as those of the lower-temperature standard oil calibrations (i.e., **Fig. A1**). These irregularities may be due to heterogeneities within the molten material. Heterogeneities include temperature gradients from the sides, bottom, and top of the crucible, as well as intermittent chunks of cooled crust that remain immersed in the melts and, at times, interact with the spindle during rotation – causing spikes in the measured torque. While these conditions cause the recorded data to be 'noisy', they are realistic in the sense that when the viscometer is deployed in active lava, thermal and physical (i.e., melt and solid crust) heterogeneities will always exist to some extent throughout these field measurements. Thus, a meticulous inspection of the data must be conducted to obtain the most reliable apparent viscosity of the material that is measured. In some cases, the torque and temperature readings may be stable for parts of the measurements but not always for the entire duration of the imposed speed ramp. One of this new device's core strengths is that all data required to scrutinize the measurement quality are recorded simultaneously and, combined with observations made during the measurements, enable carefully separating valid data from those affected by material heterogeneities. In fact, we find that there are often large portions of the measurements where no reliable data can be recovered (i.e., **Fig. A1**).

We plot and visually inspect the data collected using the matplotlib for each measurement. This is done to identify regions of moderately stable torque and temperature readings and to allow us to discard sections that display highly variable torque, and/or rapidly changing temperature because they represent non-homogenous measurement conditions. Take the data recorded for TXB run 2 (**Fig A1B**) as an example: During the entire "up" ramp in speed (green dash lines in **Fig A1B**), the data show highly unstable torque readings (red lines in **Fig A1B**) as well as

unstable, gradually increasing, temperature readings (blue lines in **Fig A1B**). Towards the end of the fastest rotation rate interval (100 rpm), both the temperature and torque readings stabilize. This is consistent with visual observations of crust becoming entrained during the insertion of the spindle (shielding the thermocouple from the "fresh" melt and creating an irregularly shaped rotating body) at the start of the measurement, which was liberated from the spindle during the fast rotation step (exposing the shear vane to "fresh" melt and reverting the rotating geometry to cylindrical). Scrutinizing the data in this way enables the user to identify and discard the early sections of the run that represent crustal spindle interactions and therefore cannot be used for reliable viscosity determinations of the lava while keeping the valuable data generated during the latter parts of the measurement.

Next, we use the *matplotlib SpanSelector* function to select the run regions that we deem stable (i.e., grey fields **Fig. A1**). The selected regions (between 270 and 488 data points) are then visually inspected again (bottom of each subplot) and, if satisfactory, the data is exported as a new .txt file and the viscosity is derived based on the calibration parameters established in **Table 1**. In some cases, the temperature gradients are never fully stable (i.e., **Fig. A1C**) despite moderately stable torque readings. The viscosities recovered from these segments of the measurements are denoted with an open-filled marker rather than a filled marker in **Figure 7**.

Figure A1: A compilation of raw data plotted for each of the six measurements conducted in the high-temperature furnace at the UB Center for Geohazards. Torque (dark red), rotational speed (green dash), and temperature (blue) are simultaneously displayed in the top portion of each subfigure. The grey fields denote the regions of selected data, based on stable reading criteria (see text). The lower portion of each subfigure shows the zoomed-in portion of raw selected data, with the same parameters and colors shown as in the top subplots.

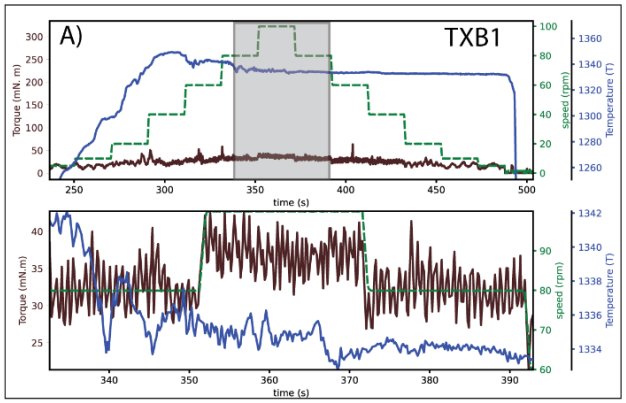
A)
TXB1
Torque (mN. m)
speed (rpm)
Temperature (T)
time (s)
Torque (mN.m)

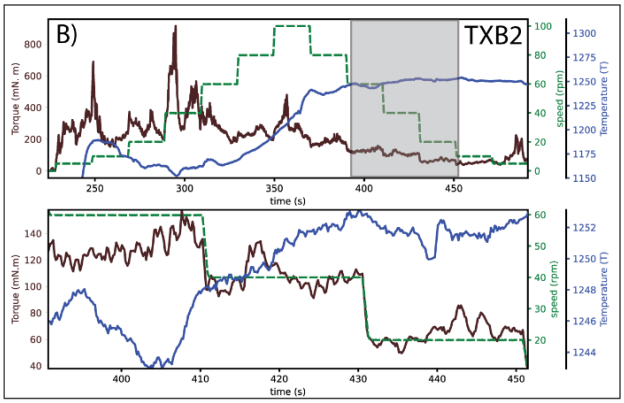
B)
TXB2
Torque (mN. m)
speed (rpm)
Temperature (T)
time (s)
Torque (mN.m)

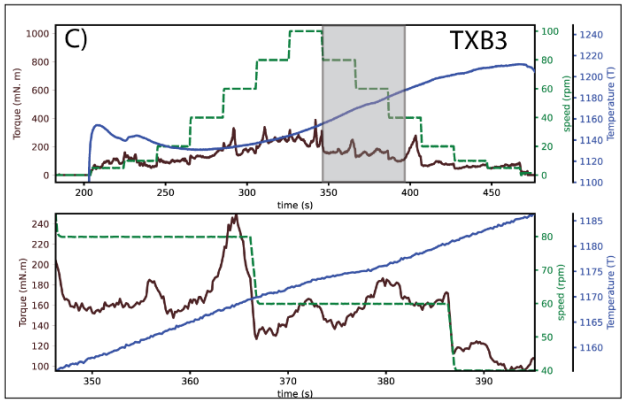
C)
TXB3
Torque (mN. m)
speed (rpm)
Temperature (T)
time (s)
Torque (mN.m)

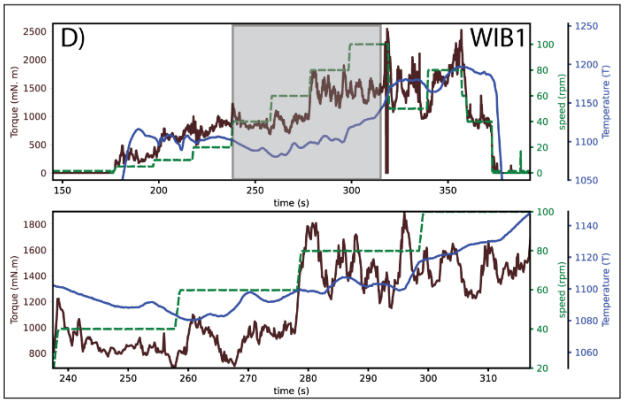
D)
WIB1
Torque (mN. m)
speed (rpm)
Temperature (T)
time (s)
Torque (mN.m)

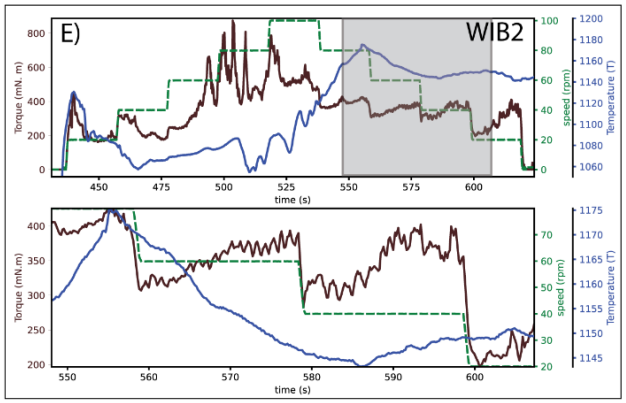
E)
WIB2
Torque (mN. m)
speed (rpm)
Temperature (T)
time (s)
Torque (mN.m)

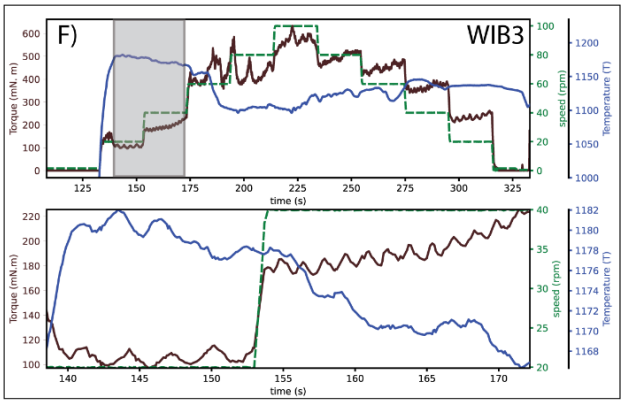
F)
WIB3
Torque (mN. m)
speed (rpm)
Temperature (T)
time (s)
Torque (mN.m)

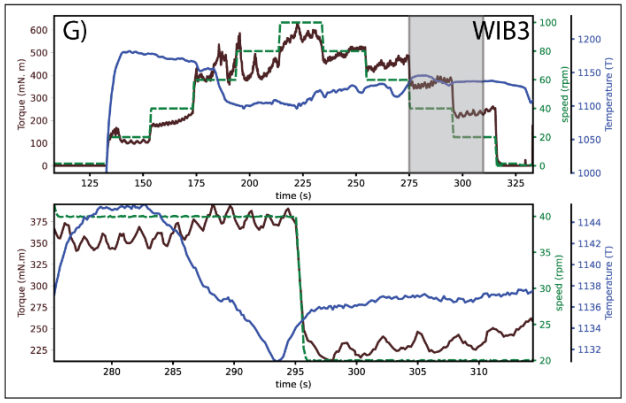
G)
WIB3
Torque (mN. m)
speed (rpm)
Temperature (T)
time (s)
Torque (mN.m)